Live-cell imaging of *Drosophila melanogaster* pupae with mesoscopic fluorescence tomography

Claudio Vinegoni, Chrysoula Pitsouli, Daniel Razansky, Norbert Perrimon & Vasilis Ntziachristos

Supplementary figures and text:

Note: Supplementary Videos 1–5 are available on the Nature Methods website.

Supplementary Figure 1: Schematic of the experimental setup.

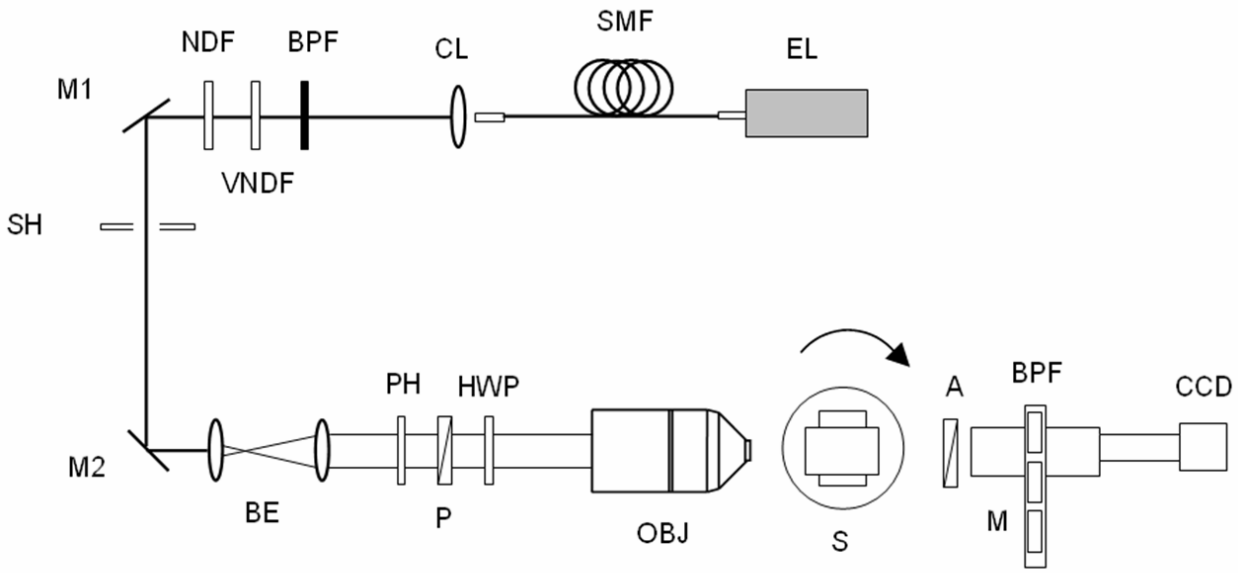

EL excitation laser, SMF single mode fiber, CL collimating lens, BPF bandpass filter, VNDF variable neutral density filter, M1,M2 mirrors, SH automatic shutter, BE beam expanding optics, PH adjustable iris, P polarizer, HWP half wave plate, OBJ focusing objective, S sample holder, A analyzer, M microscope, CCD camera.

Supplementary Figure 2: Comparison using different reconstructions schemes.

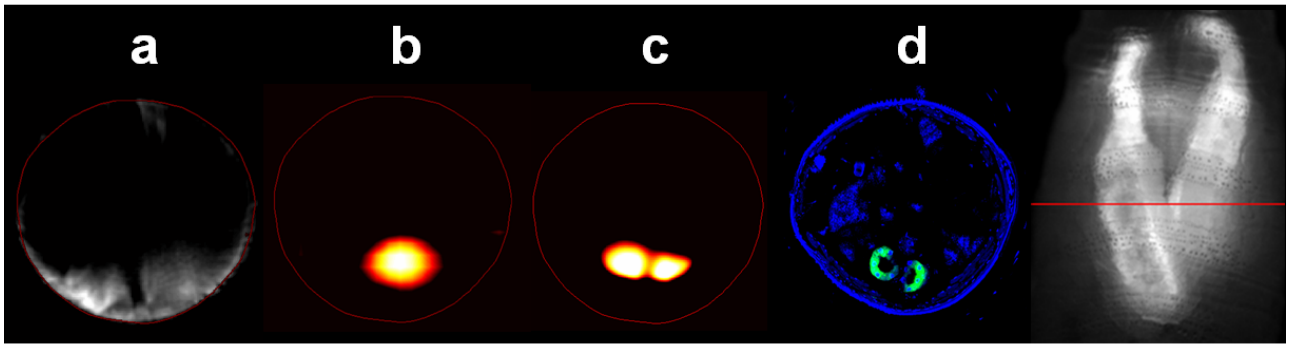

Due to the new imaging window (beyond 1 MPFL) we have investigated several reconstruction schemes in order to solve the inverse problem. Planar reconstructions of the salivary glands (**a-c**) and corresponding histology (**d**) are shown for each one of them. The simplest approach (as in Sharpe et al. 11) consists of considering a filtered backprojection or inverse Radon transform, as used in X-ray tomography. This scheme is clearly an oversimplification and it fails due to the presence of scattering as shown in (**a**). In fact light propagation can not be modeled as a pencil beam but we have to resort to a more sophisticated approach involving distribution of photon density waves within the sample. The principle of operation of diffusion optical tomography (DOT) is similar to that of X-ray computed tomography, with the distinction that DOT deals with highly scattered photons (above 10 MFP). The technique uses multiple projections and combines the measurements into an inversion schemes that accounts for high scattering. In our case the technique shows its limitation, being not able to resolve the two salivary glands.

In (c) and (d) we show a planar reconstruction using the Fermi simplification, and the corresponding histology taken from a morphologically matched area of a different pupa.

Supplementary Figure 3: GFP expression in salivary glands and CNS.

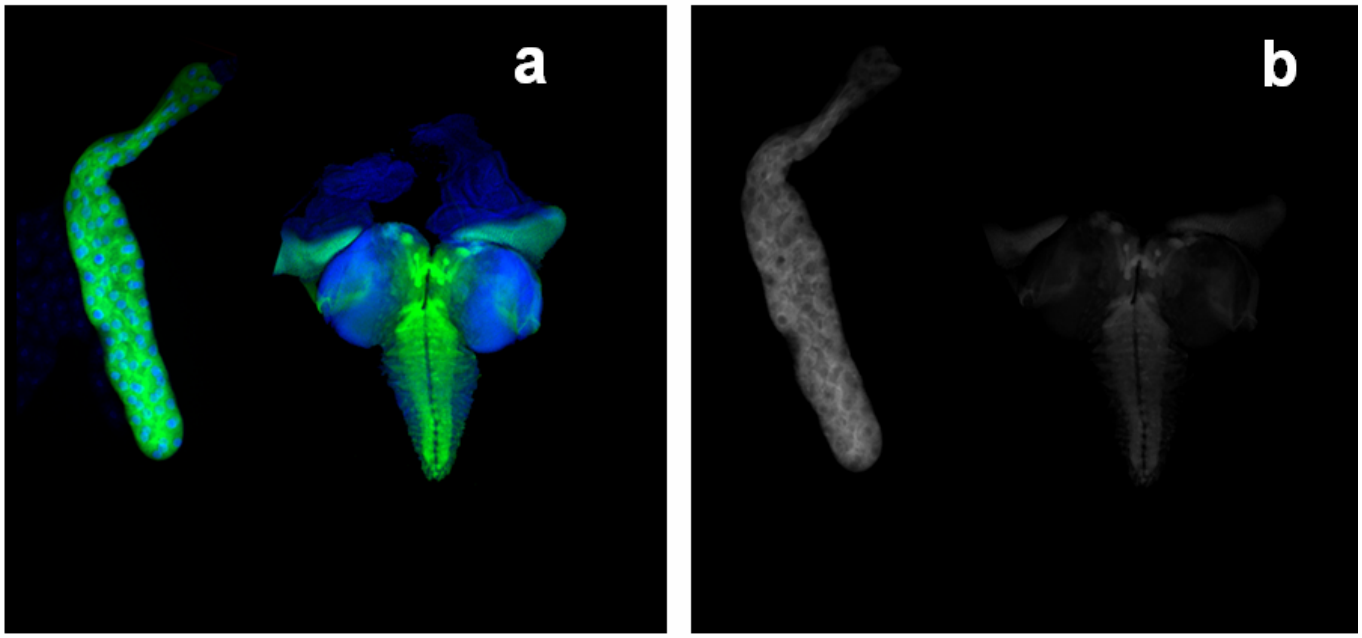

Confocal images of dissected salivary gland and CNS of a single pupa. The pupa is at a developmental stage equal to the one imaged in Fig.2. (a) CNS and salivary gland (blue, dapi staining; green, GFP fluorescence). The two organs are not on the same intensity scale (b) Fluorescence signal (GFP) only. Here, both salivary glands and CNS are shown in the same intensity scale. The signal is the sum of the total GFP fluorescence signal integrated along the axis orthogonal to the imaging plane. Although *elav-Gal4* is expressed in the nervous system, the expression level of the GFP in the CNS is clearly lower when compared to the salivary gland fluorescence.

SUPPLEMENTARY METHODS

Experimental setup and image acquisition

The experimental setup described in this work is shown in detail in **Supplementary Fig. 1**. The light source consisted of an Ar+ CW laser tuned at 488 nm. The laser served as excitation source for the GFP molecules and was filtered with a narrow band pass interference filter centered at 488 nm with a 5 nm full-width-at-half-maximum (FWHM). The light was guided with a single mode fiber and collimated using a collimating lens. A set of fixed and variable neutral density filters allowed to control the amount of light on the sample and to keep it low enough preventing GFP photobleaching and photodamage. In addition the presence of an automatic shutter allowed for long imaging sessions necessary when following the development of pupae over long periods of time.

The laser beam was then aligned with the microscope axis using two folding mirrors and then beam expanded with a combined two lenses Galilean telescope in order to fill the back aperture of a low numerical aperture objective (Olympus, PlanN 10x/0.25). Before entering the objective the beam was spatially filtered with a pinhole and linearly polarized passing through a plastic sheet polarizer (10^4:1 extinction ratio); its polarization angle was then controlled by rotating a half wave plate. Finally, the laser beam was focused in close proximity to the center area of the sample's surface. The imaged pupa was held in place on a holder and rotated along its A/P axis by way of a high speed rotation stage (Newport, PR50) with an absolute accuracy of 0.05 degrees. Three distinct manual controllers allow for the pupa's A/P axis to be tilted and adjusted in its orthogonal plane.

The fluorescent GFP signal from the pupa was filtered through a narrow band-pass interference filter with center frequency at 513 nm and with a 5 nm FWHM, coupled with a 502 nm longpass filter (Omega. Optical, Brattleboro, VT) and collected with a Leica microscope consisting of a Z16 APO. The filters can be easily interchanged for use with different selected fluorophores. An analyzer in front of the microscope selected photons with their polarization parallel to the incident ones, a process which rejected highly diffusive photons (~10% of the photons collected)

The fluorescence images were acquired with a CCD (Pixel Fly QE) with a pixel array of 1392x1024 (pixel size 6.5x6.5 mum), 12-bit dynamic range, and a quantum efficiency up of about 50%.

Image Reconstruction

To accurately determine the forward model necessary for accurate inversion, the three-dimensional pupa surface was computed for each pupa imaged, using surface capture techniques described in Ripoll et al.[1]. This was based on contours generated using the outline of the pupa detected at each of the 180 angle projections. Surface computation allows the determination of the exact projection of each CCD pixel in relation to the pupa's surface and facilitated calculations of the intersection points of each detector with the pupa surface in each projection. Consecutively the main of light propagation from the intersection point on the surface towards the inner volume of the pupa is calculated using Snell's law of optical refraction, while assuming $n = 1.33$ index of refraction inside the pupa as appropriate for visible light wavelengths. The Fermi function of light distribution was then computed in this direction and was applied to describe the forward-peaked light diffusion within the pupa. By applying the same procedure for the 300 x 300 CCD detector elements, accurate propagation description (Green's functions) for the photons collected by the different virtual detectors (CCD pixels) employed were constructed. The Green's function, describing the light propagation of the excitation light within pupa, was constructed by mapping the laser beam onto 300 x 300 virtual point sources assumed on the pupa surface and a corresponding propagation using the Snell's correction and Fermi distribution was assumed also for each virtual source element. The resulting 300 x 300 fields were summed together to provide a single map of excitation light intensity (source Green's function) within the pupa. To obtain the final 3D fluorescence reconstruction, the fluorescence distribution, detected by the CCD at each angle projection and surface point, was backprojected onto a three-dimensional 300 x 300 x 300 mesh, after normalization by the product of the two Green's functions described above, calculated on the same 300 x 300 x 300 grid. The object's mesh was subsequently rotated 180 times (per each angle projection) and the backprojected values were summed up in each projection to constitute the final reconstructed image. Typical volumes considered in the inversion

were 1.2 x 1.2 x 1.2 mm^3. Inversions required approximately 50 seconds for surface computation and 40 minutes for 3D image reconstruction on a Pentium 4 workstation.

The diffusion approximation to the transport equation has been overwhelmingly used for in-vivo optical imaging of > 10 mm thick tissues, a length scale at which the condition $L >> l_t$ is satisfied, with L the thickness of the medium and l_t the transport mean free path i.e. the distance a photon travels before it becomes completely diffused. However, due to the aqueous, semi-transparent nature of the developing *D. melanogaster* pupa, other simplified solutions to the transport equation that retain a strongly forward propagation component (asymmetry parameter *g*, defined as the mean cosine of the scattering angle, $g \approx 1$) appear more appropriate. Such solutions have been derived for modeling light propagation in low scattering media based on the Fokker-Plank or the Leakens-Larsen approximation, which assume strong forward peaked scattering and $L>l_t$ [2,3], and the Fermi approximation, the latter assuming forward peaked scattering and $L \leq l_t$ [4]. While the Fokker Plank and the Leackens-Larsen can be viewed as the leading term in an asymptotic expansion of the linear Boltzman equation[5] the Fermi assumption in turn, which operates at a narrower propagation regime, can be viewed as the asymptotic limit of the Fokker-Plank equation for $\sigma_{tr}L \rightarrow 0$, and as the asymptotic limit of the transport (linear Boltzman) equation for $\sigma_{tr}L \rightarrow 0$ and $\sigma_t L \rightarrow \infty$ (here $\sigma_{tr}^{-1}$and σ_t^{-1} represent the transport mean free path and the mean free path respectively)[4]. To confirm whether this simpler of assumptions would suffice for imaging the developing *D. Melanogaster* pupa, we performed experimental measurements shown in **Fig. 1** where a fluorochrome of finite volume was inserted in the pupa in order to track the spatial distribution of photons as a function of depth. In this case the utilization of the Fermi equation demonstrated good agreement with the experimental data equation (curve in **Fig. 1d** fitted with a transport cross section $\sigma=0.43$ mm^{-1} into off-axis data points), which was further corroborated by the significant improvement over reconstructions based on pencil-beam or diffusion-based inversion models, as shown in **Supplementary Fig. 2**. It is expected however that as the ratio of the diameter of the organism imaged over the mean-free path-length increases, the selection of solutions to mathematical models that more closely approximate the radiative transport equation, such as solutions to the Fokker-Planck or Leakeas-Larsen equations, would be necessary[2].

Detection Sensitivity

While fluorescence is a highly sensitive method, true tomographic sensitivity depends not on the absolute photon detection sensitivity but on the contrast achieved between the imaging target and the background or other neighboring fluorescent structures. For example the presence of fluorescently labeled large structures together with smaller ones (as is the case here when imaging GFP-expressing salivary glands and the Central Nervous System (CNS)/eye discs) could lead to some problems due to the fact that diffusion of the signal coming from the salivary glands could hide the signal coming from the smaller ones (CNS/eye discs), present deeper within the pupa.

This does not imply that fluorescently labeled small structures can not be reconstructed in the presence of the larger ones. In fact, this can be achieved for example by multispectral imaging. The current availability of fluorescent proteins in the different parts of the optical spectrum, allows to image simultaneously different biological structures with each one marked with a distinct fluorescent protein. This multispectral approach could be easily implemented in our system, allowing us to monitor and resolve the development of different organs within the same pupa.

Finally we want to emphasize that even Förster resonance energy transfer (FRET) imaging, commonly used for studying protein interactions, could be a potential application for our method. Recently FRET-based caspase indicators, which are monitoring apoptotic cell death, have been used to investigate spatiotemporal analysis of in vivo caspase activation during apoptosis in the metamorphosing salivary glands[6]. It is anticipated that tomographic 3D time-lapse imaging of these tissues could alleviate the need of in vitro cultures and hormonal induction of the glands.

To experimentally resolve the issue of sensitivity in the current method as applied herein, we collected confocal images (see **Supplementary Fig. 3**) of dissected salivary glands and CNS from the same pupa at a stage equal to the one imaged and reconstructed in **Fig. 2** of the manuscript. **Supplementary Fig. 3a** shows both CNS and salivary glands on different intensity scales (blue, dapi staining; green, GFP fluorescence). **Supplementary Fig. 3b** shows the GFP fluorescence signal only for both CNS and salivary glands plotted on the same scale. Here, the signal is the sum of the total GFP fluorescence

signal integrated along the axis orthogonal to the imaging plane. Although *elav-Gal4* is expressed at high levels in the nervous system, as clearly seen the expression level of the GFP in the CNS is clearly smaller than in the salivary glands.
The tomographic reconstructions of **Fig. 2b,c** are actually taken above and below the CNS/eye discs. As for **Fig. 2d** due to the sensitivity issue mentioned above, the tomographic reconstructions are thresholded such that only the salivary glands are evident.

Specimen preparation

Larvae were collected and monitored for pupariation in order to image the white prepupal stage. To avoid the background fluorescent signal caused by the fly food and the salivary gland glue, all the animals were washed with PBS for several minutes using a moist paintbrush. After the cleaning procedure, no fluorescence background was recorded in wild-type animals.

For stability purposes the animals are held firmly in place by inserting their posterior end into a capillary glass (internal diameter ca. 800 microns), while the imaged part is exposed outside of the capillary. The capillary glass is then vertically fixed on the rotation stage and its axis adjusted in order to avoid any precession.
During acquisition the animals are maintained in a relative high humidity environment at an ambient temperature of about 25^0 C. Under these conditions most of the animals developed normally through metamorphosis with head eversion occurring about 12 h after puparium formation.

While it is possible to image different cells in the *D. Melanogaster* pupa by cutting a small window into the pupal case, this practice is only implemented at later developmental stages (later than 12 hours after puparium formation (APF)). At this late stage the pupal epidermis is detached from the pupal case, which allows for the removal of the latter without damaging the animal structure[7]. Since our work focuses on imaging pupae at an early stage, it is imperative to leave the pupal case intact so as to perform measurements in an unperturbed environment. The experience we gained with working at this early stage showed that even minor resection significantly altered the mechanical strength of the pupal case, resulting in the loss of fluids by the pupa and the eventual change of shape, size and internal composition leading eventually to non-surviving insects.

Drosophila strains

Drosophila melanogaster stocks used in this study are all described in Flybase (www.flybase.org)
elav-Gal4 (FBti0002575)
ap-Gal4^{md544} (FBal0051787)
UAS-srcEGFP (FBti0013990)
w^{1118} (FBal0018186)
Flies were kept at 25C on standard food medium

The *Gal-4/UAS* system[8] was used in order to express GFP tissue-specifically in the pupae. All crosses were kept at 25^0C.

For imaging of the salivary glands, *elav-Gal4/+; UAS-srcEGFP/+* animals were used. The *elav-Gal4* driver is expressed in the whole nervous system[9] and the salivary glands. Since the expression in the latter is very strong, imaging was focused on those.

Imaging of the discs was performed in *ap-Gal4 UAS-srcEGFP/+* animals. *ap-Gal4* marks the dorsal compartment of imaginal discs[10]. The dorsal compartment of each wing disc will give rise to the dorsal surface of the adult wing and half of the thorax.

Histology and confocal microscopy of *D. Melanogaster* pupae

The pupal case of white prepupae (0 hrs After Puparium Formation) was pricked twice with a fine needle (insect pin 000, FST) before fixation. Pupae were fixed in 8% Formaldehyde, 1x PEM (100mM Pipes, 1mM EGTA, 1mM $MgCl_2$) for 6-8 hrs at room temperature with gentle agitation. After removal of fixation and rinsing with 1x PBS, a sharp blade was used to cut the fixed pupa in two pieces perpendicular to the A/P axis; these were submerged in Vectashield with dapi (Vector) and subsequently mounted on coverglass slides (Lab-Tek) for imaging. Images were acquired using an inverted Leica DM IRE2 confocal microscope.

White prepupae were collected and staged accordingly in humid chambers, when different developmental stages were analyzed.

Dissections of salivary glands and CNS/eye discs were performed in 1x PBS. Tissues were fixed in 4% Formaldehyde, 1x PEM for 20min at room temperature. After removal of fixation, tissues were mounted in Vectashield with dapi (Vector) and imaged on a Leica TCS NT2 AOBS microscope.

SUPPLEMENTARY REFERENCES

1. Ripoll J., Schultz R. B., and Ntziachristos V. *Phys. Rev. Lett.* **91**, 103901 (2003).
2. Kim, A. D. & Moscoso, M. *J. Opt. Soc. Am. A* **21**, 797-803 (2004).
3. Kim, A. D. & Keller, J.B. *J. Opt. Soc. Am. A* **20**, 92-98 (2003).
4. Borgers, C. & Larsen, E.W. *Proc. Int. Conf. Math. and Computation* (1995).
5. Borgers, C. & Larsen, E. W. *Med. Phys.* **23**, 1749-759 (1996).
6. Takemoto, K. et al. *Proc. Natl. Acad. Sci. USA.* **104**, 13367-72 (2007).
7. Nivov, N., Chiarelli, D. A., & Martin-Blanco, E. *Development* **134**, 367-79 (2007).
8. Brand, A., and Perrimon, N. *Development* **118**, 401-405 (1993).
9. Lin, D.M., Goodman, C.S. *Neuron* **13**, 507-523 (1994).
10. Diaz-Benjumea F.J. and Cohen S.M. *Cell* **75**, 741-52 (1993).